

Swift XRT Observations of the Nova-like Cataclysmic Variables MV Lyr, BZ Cam and V592 Cas

Şölen Balman

Department of Physics, Middle East Technical University, Ankara, Turkey

`solen@astroa.physics.metu.edu.tr`

and

Patrick Godon¹, Edward M. Sion

*Astronomy & Astrophysics, Villanova University,
800 Lancaster Avenue, Villanova, PA 19085, USA*

`patrick.godon@villanova.edu, edward.sion@villanova.edu`

ABSTRACT

We present a total of ~ 45 ksec (3×15 ksec) of *Swift* XRT observations for three non-magnetic nova-like (NL) Cataclysmic Variables (CVs) (MV Lyr, BZ Cam, V592 Cas) in order to study characteristics of Boundary Layers (BL) in CVs. The nonmagnetic NLs are found mostly in a state of high mass accretion rate ($\geq 1 \times 10^{-9} M_{\odot} \text{ yr}^{-1}$) and some show occasional low states. Using the XRT data, we find optically thin multiple-temperature cooling flow type emission spectra with X-ray temperatures (kT_{max}) of 21-50 keV. These hard X-ray emitting boundary layers diverge from simple isobaric cooling flows indicating X-ray temperatures that are of virial values in the disk. In addition, we detect power law emission components from MV Lyr and BZ Cam and plausibly from V592 Cas which may be a result of the Compton scattering of the optically thin emission from the fast wind outflows in these systems and/or Compton up-scattering of the soft disk photons. The X-ray luminosities of the (multi-temperature) thermal plasma emission in the 0.1-50.0 keV range are $(0.9-5.0) \times 10^{32} \text{ erg/sec}$. The ratio of the X-ray and disk luminosities (calculated from the UV-optical wavelengths) yield an efficiency (L_x/L_{disk}) $\sim 0.01-0.001$. Given this non-radiative ratio for the

¹Visiting in the Henry A. Rowland Department of Physics and Astronomy, The Johns Hopkins University, Baltimore, MD 21218.

X-ray emitting boundary layers with no significant optically thick blackbody emission in the soft X-rays (consistent with *ROSAT* observations) together with the high/virial X-ray temperatures, we suggest that high state NL systems may have optically thin BLs merged with ADAF-like flows and/or X-ray coronae. In addition, we note that the axisymmetric bipolar and/or rotation dominated fast wind outflows detected in these three NLs (particularly BZ Cam and V592 Cas) or some other NL may also be explained in the context of ADAF-like BL regions.

Subject headings: binaries:close - accretion, accretion disks - cataclysmic variables
- white dwarfs - stars:individual(MV Lyr, BZ Cam, V592 Cas)

1. Introduction

Cataclysmic Variables (CVs) are short period (up to ~ 2 day) close binary systems in which a white dwarf (WD) accretes matter from a late-type main sequence star filling its Roche lobe (Warner 1995). In non-(or weakly-) magnetic CVs the transferred material forms an accretion disk around the WD and reaches all the way to the stellar surface, as the magnetic field is not strong enough to disrupt the accretion disk.

NL systems are a class of CVs usually found in a state of high mass accretion rate, though some NLs are sometimes found in a low state of reduced accretion. NLs have two main subclasses where VY Scl stars exhibit high states and occasional low states of optical brightness and the UX UMa stars remain in the high state and low states are not seen (Warner 1995). RW Tri stars are NLs that are eclipsing UX UMa systems (so they're all high inclination NLs). While all NL variables show emission lines, UX UMa sub-type of NLs also exhibit broad absorption lines in the optical and/or UV wavelengths. In the high states of NLs, the accretion rates are typically a few $\times 10^{-8} M_{\odot} \text{ yr}^{-1}$ to a few $\times 10^{-9} M_{\odot} \text{ yr}^{-1}$. Virtually all NLs reside above the period gap with a concentration of them between P_{orb} of 3 and 4 hours (Ritter & Kolb 1998). There is only one NL below the period gap (BK Lyn), this system has been identified with a nova in ancient times from chinese records (see Patterson et al. 2013). The high accretion rates are inferred from luminous disks seen best and modeled in the FUV with steady-state disk models. In addition, bipolar outflows and/or rotationally dominated winds from NLs are detected primarily in the FUV, and P Cygni profiles of the resonance doublet of CIV are almost invariably seen from these collimated outflows in systems with disk inclinations less than 60-70 degrees (Guinan & Sion 1982, Sion 1985). The high accretion rates may be driven in part by irradiation of the donor star if the accreting WD remains hot (e.g., long after a nova event). Existence of hot WDs in NLs in turn leads to irradiation of the donor hence a driving of the high mass transfer by the donor, either by

irradiation driving a wind off of the donor or by irradiation causing the Roche-Lobe filling donor star to be bloated. There is another subclass of nonmagnetic CVs called SW Sex stars often listed as part of NLs. These are defined by specific spectroscopic characteristics and have orbital periods between 3-4 hrs (see Rodriguez-Gil et al. 2007 for a review). Not all NLs show these characteristics. Our present paper does not deal with SW Sex stars.

Observations of CV disk systems at low mass accretion rate (namely dwarf nova CVs in quiescence) have successfully led to the determination of the temperature and luminosity of the accreting white dwarfs from FUV observations (where it is the dominant emitting component at low \dot{M}) and X-ray observations have yielded the temperature and luminosity of the optically thin BLs. The dwarf novae in quiescence (low \dot{M} systems) were observed with recent X-ray telescopes like *XMM-Newton*, *Chandra*, and *Suzaku* (e.g. Szkody et al. 2002, Pandel et al. 2005, Rana et al. 2006, Okada et al. 2008, Ishida et al. 2009, Mukai et al. 2009, Balman et al. 2011) and the results seem in accordance with one-dimensional numerical simulations of the optically thin BLs in standard steady-state disks of DNe in quiescence with low accretion rates (10^{-10} - 10^{-12} M_{\odot} yr^{-1} , (Narayan & Popham 1993, Pringle 1981). However, note that a recent study of X-ray variability and inner disk structure of DN in quiescence reveals optically thick disk truncation and plausible formation of hot (coronal) flows in the inner parts of the quiescent DN accretion disks (Balman & Revnivtsev 2012).

One of the earliest comprehensive studies on hard X-ray emission from the boundary layers of CVs using the *Einstein* IPC (0.2-4 keV) indicate that NL systems (5 detected systems) emit hard X-ray emission in this range with luminosities \leq a few $\times 10^{32}$ erg s^{-1} (Patterson & Raymond 1985). NL systems have been detected in the early epochs of *ROSAT* Observatory (about 11 NL systems; 0.1-2.4 keV) and optically thick soft X-ray components expected from these high accretion rate systems are not detected (van Teeseling et al. 1996). For these systems a hot optically thin X-ray source is found with plasma temperatures $kT < 6$ keV. The X-ray luminosities are $<$ a few $\times 10^{32}$ erg s^{-1} whereas the UV luminosities are in a range 10^{31} - 10^{35} erg s^{-1} . In addition, Greiner (1998) has done a comprehensive analysis of the *ROSAT* detected NLs (see also Schlegel & Singh 1995) and have argued that *ROSAT* data are also consistent with blackbody models yielding lower χ^2_{ν} than thermal plasma models. These blackbody temperatures are calculated as (0.25-0.5) keV with very small emitting regions. Later, some NLs were studied with *ASCA* and are found consistent with double MEKAL models at different temperatures (e.g., TT Ari and KT Aur, Mauche & Mukai 2002), and one with *XMM-Newton* using multiple-temperature plasma and MEKAL models (Pratt et al. 2004). In all these observations the X-ray luminosities are \leq a few $\times 10^{32}$ erg s^{-1} .

Recent advances in UV spectroscopy have revealed that the high mass accretion disks in nova-likes are departing from the standard disk models especially in the inner disk (Puebla et

al. 2007), where the boundary layer is, also, located. Puebla et al. (2007) have done a comprehensive UV modeling of accretion disks at high accretion rates in 33 CVs including many NLs and old novae. The UV findings indicate a necessity for improvement by incorporating a component from an extended optically thin region (e.g., wind, corona/chromosphere). This is evident from the strong emission lines and the P Cygni profiles observed in the UV spectra. Disk irradiation by the boundary layer or the central star, and nonstandard temperature profiles would help for better modeling in this band. An additional possibility to explain model discrepancies is disk truncation. Yet another possibility is to modify the viscosity law for example by using constraints on the viscosity following from numerical simulations of the magneto-rotational instability. A first step in improving the disk modeling has been to modify the inner disk to reflect the presence of a hot boundary layer (e.g. for QU Car: Linnell et al. 2008; for MV Lyr: Godon & Sion 2011) where an additional hot optically thick component was also found consistent with the data when modeling in the UV.

2. The Nova-like Systems MV Lyrae, BZ Camelopardalis, and V592 Casiopeiae

In this paper, we present the *Swift* XRT observations of three NLs, MV Lyr, BZ Cam, and V592 Cas. The important characteristics of the systems are presented in Table 1 and the relevant literature is summerized below.

2.1. MV Lyr

MV Lyrae is a member of VY Scl subclass of NLs, mostly found in a a high state of accretion (similar to the outburst state of DNs but lasting much longer) with occasional drops (short-duration) in brightness. In these low states, the magnitude of MV Lyr drops from $V \approx 12 - 13$ to $V \approx 16 - 18$ (Hoard et al. 2004). The archival AAVSO data reveals that it stays in a high state for up to ~ 5 yr, and following that for a period of a few years to ~ 10 yr it starts alternating between high state and low state on a time scale of a few months to a year. MV Lyrae has an orbital period of $P = 3.19$ hr and a mass ratio of $q = M_{2nd}/M_{wd} = 0.4$ (Schneider et al. 1981; Skillman et al. 1995). The inclination of the system is found in a range $i = 10^\circ - 13^\circ$, constrained with the small radial velocity measurements and lack of eclipses (Linnell et al. 2005).

The UV observations of MV Lyr obtained with the *International Ultraviolet Explorer* (*IUE*) during its low state revealed the existence of a hot WD reaching 50,000K (Szkody & Downes

1982) or higher (Chiappetti et al. 1982). Later, the source was observed in a different low state with *FUSE* (in 2002) that lasted about 8 months. The analysis showed that the WD has a temperature of 47,000K, a gravity of $\log g = 8.25$, a projected rotational velocity of $V_{rot} \sin i = 200 \text{ km s}^{-1}$, sub-solar abundances of $Z = 0.3 \times Z_{\odot}$, and a distance of $505 \pm 50 \text{ pc}$ (see Hoard et al. (2004)). In this low state, the magnitude of MV Lyr was around $V \approx 18$ with a mass accretion rate about $\dot{M} \approx 3 \times 10^{-13} M_{\odot} \text{ yr}^{-1}$ (Hoard et al. 2004). Furthermore, Linnell et al. (2005) studied the different states of MV Lyr and its secondary with the aid of *IUE* and HST/*STIS* spectra, and found that the mass accretion rate was of the order of $3 \times 10^{-9} M_{\odot} \text{ yr}^{-1}$ during the high state. (Godon & Sion 2011) analyzed the FUSE spectrum of MV Lyr in its high state and found an accretion rate of about $2 \times 10^{-9} M_{\odot} \text{ yr}^{-1}$, assuming $i = 10^{\circ} \pm 3^{\circ}$ (Schneider et al. 1981; Skillman et al. 1995; Linnell et al. 2005), a 50,000K WD and an extended 100,000K UV emitting region which can originate from an optically thick BL or it can be from an inner disk region irradiated by the boundary layer (i.e., optically thin BL).

2.2. The Peculiar Nova-like BZ Cam

BZ Cam is a peculiar NL with rather special characteristics among cataclysmic variables. First, it is associated with a bow-shock nebula (Ellis et al. 1984; Krautter et al. 1987; Greiner et al. 2001); second, as a wind-emitting system it manifests its outflow not only in the FUV resonance lines (as do wind-emitting CVs) but also in the Balmer and He I lines (Patterson et al. 1996); third, the wind shows a bipolar nature as a highly unsteady and continuously variable $\sim 3000 \text{ km s}^{-1}$ supersonic outflow (Honeycutt et al. 2013); last, the variability timescales seen in its optical wind-outflow features are much shorter (minutes to hours) than the shortest variability reported in the FUV of any other CV wind (Patterson et al. 1996).

For these reasons, BZ Cam has been the subject of many studies of the time-variability of its line profiles (e.g. (Krautter et al. 1987; Hollis et al. 1992; Woods et al. 1992; Griffith et al. 1995; Prinja et al. 2000; Honeycutt et al. 2013)). It is classified as a VY Scl type NL system with a period of 221 min (Thorstensen et al. 1993; Patterson et al. 1996). Garnavitch & Szkody (1988); Greiner et al. (2001) present an analysis of its two optical low states. The source has an inclination of about $i = 12^{\circ} - 40^{\circ}$ (la Dous 1991; Ringwald & Naylor 1998) and a distance of $830 \pm 160 \text{ pc}$.

Its WD mass is unknown but it is thought to contain a $0.3 - 0.4 M_{\odot}$ main-sequence donor star (Lu & Hutchings 1985). It is mostly seen at a magnitude of $V = 12.0 - 12.5 \text{ mag}$ and during low state reaches $V = 14.3 \text{ mag}$ (Greiner et al. 2001). It was observed

with ROSAT (van Teeseling et al. 1996), IUE (Krautter et al. 1987; Woods et al. 1990, 1992; Griffith et al. 1995), HST/GHRS (Prinja et al. 2000) and FUSE (Froning et al. 2012). The UV and optical continuum is consistent with a $\sim 12,500$ K Kurucz LTE model atmosphere (Prinja et al. 2000) with a small emitting area compared to the surface of a WD. In work presented elsewhere (Godon et al. 2014, in preparation), our analysis of the archival FUSE spectra of BZ Cam reveals a 50,000 K WD.

2.3. V592 Cas

V592 Cas is an UX UMa subtype of Nova-like with an inclination of $i = 28^\circ \pm 10^\circ$ (Huber et al. 1998), and a period of 2.76 hr (Taylor et al. 1998). With a reddening of $E(B-V)=0.22$ (Cardelli et al. 1989), it has been placed at about 330-360 pc (Huber et al. 1998; Hoard et al. 2009). Its WD is about $0.75 M_\odot$ with a temperature of 45,000 K (Hoard et al. 2009) and a mass accretion rate around $1 \times 10^{-8} M_\odot \text{ yr}^{-1}$ (Taylor et al. 1998; Hoard et al. 2009). V592 Cas has a bipolar wind outflow that has an episodic nature, with several events reaching velocities of 5000 km s^{-1} in $H\alpha$ where the optical brightness variations and the strength of the outflow reveals no clear correspondance (Kafka et al. 2009). V592 Cas was observed with IUE (Taylor et al. 1998) and FUSE (Prinja et al. 2004) revealing Doppler shifts of the entire blueward absorption troughs in the ultraviolet resonance lines as the main source of variability characterized with an asymmetric and non-sinusoidal behaviour over the orbital phase. Furthermore, the outflowing wind does not show modulated variation on the superhump periods detected from V592 Cas, but show modulation only on the orbital phase (orbital period). This indicates that neither the precession of the disk nor the precession of the disk tilt (negative and positive superhumps) is affecting the outflow. In addition, V592 Cas reveals a short photometric oscillation of 22 mins (Kato 2002).

3. The Standard Star-Disk Boundary Layer

The standard disk theory (Shakura & Sunyaev 1973; Lynden-Bell & Pringle 1974), predicts that viscous dissipation of energy is instantly radiated locally in the vertical z-direction. The disk total luminosity L_{disk} is half the accretion luminosity

$$L_{disk} = \frac{L_{acc}}{2} = \frac{GM_*\dot{M}}{2R_*}, \quad (1)$$

where G is the gravitational constant, M_* is the mass of the accreting star, R_* its radius and \dot{M} is the mass accretion rate. Each face of the disk radiates $L_{disk}/2$.

If the star is not rotating close to breakup (i.e. $\Omega_* \ll \Omega_K(R_*)$), then the theory predicts (e.g. Pringle (1981)) that the remaining rotational kinetic energy of the material at the inner edge of the disk (rotating at the local Keplerian speed) is dissipated in a small region as this material lands on the WD which is rotating more slowly at sub-Keplerian speeds. This region is referred as the boundary layer (BL) and up to half the accretion luminosity is liberated in this region. This remaining rotational kinetic energy given-off from the BL (L_{BL}) is (Kluźniak 1987):

$$L_{BL} = L_{disk} \left(1 - \frac{\Omega_*}{\Omega_K(R_*)} \right)^2. \quad (2)$$

The BL luminosity is not reduced more than a factor of 1/4 due to rotational effects. At high mass accretion rates ($\dot{M} \approx 10^{-9} - 10^{-8} M_\odot \text{ yr}^{-1}$) the BL is largely expected to be optically thick and emits in the soft X-ray band (Pringle 1977; Pringle & Savonije 1979; Popham & Narayan 1995; Godon et al. 1995; Hertfelder et al. 2013), and at lower mass accretion rates it is expected to be optically thin and emit in the hard X-ray ($\sim 10 \text{ keV}$) band (Narayan & Popham 1993, Popham 1999). Furthermore, two-dimensional semi-analytical work (Piro & Bildsten 2004) shows that effects of the centrifugal force and pressure may result in, rings of enhanced brightness above and below the WD equator, called the “spreading layer” (Inogamov & Sunyaev 1999). At lower mass accretion rates than $< 1.6 \times 10^{-8} M_\odot \text{ yr}^{-1}$, however, Piro & Bildsten (2004) shows that the spreading is negligible which is the case for the three NL sources in this paper (see Table 1 for the accretion rates). The transition between an optically thin and an optically thick boundary layer does not only depend on the mass accretion rate, it also depends on the mass of the white dwarf, on its rotational velocity, and on the alpha viscosity parameter (disk viscosity $\nu = \alpha c_s H$ where c_s is the sound speed, H is the disk height and α is a free parameter in a range 0-1).

4. Observations and Data

Swift was launched in November 2004 (Gehrels et al. 2004) mainly designed to measure position, spectrum and brightness of gamma-ray bursts (GRBs). It has a Burst Alert Telescope (BAT; Barthelmy et al. (2004)) with typically 100 sec reaction time and a field of view (FOV) of $100^\circ \times 60^\circ$ working in 15-150 keV range using a CdZnTe CCD. The narrow field instruments are the X-ray telescope (XRT; Burrows et al. (2005)) and the Ultraviolet-Optical Telescope (UVOT; Roming et al. (2005)). The XRT operates in the 0.2-10 keV range with an 18 arcsec half-power diameter at 1.5 keV using CCDs that are similar to EPIC MOS on *XMM-Newton*. It has an FOV of 23.6×23.6 arcmin and an imaging resolution of 2.4 arcsec per pixel. Regular observations of MV Lyr, BZ Cam and V592 Cas were made

with the *Swift* spacecraft between 2012 June 8 and 2012 December 21 utilizing both the XRT and the UVOT using the UV grism. Table 2 gives the details and log of the observations. In this paper, we report on the analysis of the XRT data of the three NLs obtained in the photon counting (PC) mode for about 15 ksec each. Data were obtained, also, in the windowed timing mode (WT) using short exposures less than 5 min, this mode does not provide spatial resolution. Such short exposure times will not yield adequate S/N for any spectral or timing analysis, thus WT data have not been used for the analysis. The UV grism analysis will be discussed in a subsequent paper. PC mode is a frame transfer operation of an X-ray CCD retaining full imaging and spectroscopic resolution, but the time resolution is only 2.5 sec; the mode is used at low fluxes below 1 mCrab. We find XRT count rates of 0.069(3) c s⁻¹ for MV Lyr, 0.051(2) c s⁻¹ for V592 Cas, and 0.070(3) c s⁻¹ for BZ Cam. We cross checked the states of the sources using the existing AAVSO data and the UVW1 filter magnitudes and count rates, obtained simultaneously with the PC mode data. We find that all the three NLs were in a high state during the *Swift* observations.

The screened and pipeline-processed data (aspect-corrected, bias-subtracted, graded (0-12) and gain-calibrated event lists) are used for the analysis. Latest calibration file on the *Swift* database (version, 20010101v013) is used, in accordance with the XRT data for the redistribution matrix. The ancillary response files are calculated for each source by merging exposure maps in XIMAGE created using *xrteexpomap* task and finally running the task *xrtmkarf*. For light curve and spectrum generation, and further analysis, XSELECT V2.4b and HEASoft 6.13 (see <http://heasarc.nasa.gov/lheasoft/>) are utilized.

In addition, we have used *ROSAT* archival data of our target sources to derive black-body temperature upper limits. The data for MV Lyr was obtained on 1992 November 4-8 using the PSPCB detector (20 ksec); OBSID rp300192n00. For BZ Cam, the observation was performed on 1992 September 28-29 using the PSPCB detector (6.0 ksec); OBSID rp300233n00. Finally for V592 Cas, the data was obtained during the RASS (all sky survey; 1990 December 29 to 1991 August 06) using the PSPCC detector (0.6 ksec); OBSID rs930701n00. The three *ROSAT* data sets were acquired in high states, note that V592 Cas is a UX UMa type of NL which shows only high states. For details of *ROSAT* data see van Teeseling et al. (1996), Greiner (1998), and Voges et al. (1999).

5. Temporal Analysis

XRT light curves are extracted from the data sets of each NL sampling between 0.2-10 keV at 2.7 sec resolution and background subtracted. A circular region of radius 1.5 arc min is used for the photon extraction for both the source and the background (devoid of other

contaminating sources).

We searched for variations of the X-ray light curves over the orbit of the systems by folding each light curve on the orbital period using 10 phase bins. The results are displayed in Figure 1. For the orbital periods we used the spectroscopic periods derived for the three NLs: (1) For BZ Cam, we used the period and the ephemeris derived from the He I $\lambda 5876$ line ($T_0=2453654.008(2)+0.15353(4)\times E$; Honeycutt et al. 2013); (2) For V592 Cas, we used the ephemeris derived from the He I $\lambda 5876$ and $\lambda 6678$ line ($T_0=2450707.866(1)+0.115063(1)\times E$; Taylor et al. 1998); (3) For MV Lyr, we used the ephemeris derived from the $H\alpha$ line ($T_0=2449258.05+0.1329(4)\times E$; Skillman et al. 1995). In Figure 1 each NL shows some variation of the X-ray count rates over the orbit of the system. V592 Cas shows complex behaviour, but looks in-phase with the $H\alpha$ variation (only the first narrow X-ray peak) and possibly out-of-phase with the He I $\lambda 5876$ line. Both in BZ Cam and V592 Cas, the He I $\lambda 5876$ line and $H\alpha$ line variations are out-of-phase. V592 Cas shows dips close to zero counts per sec and the X-ray variations seem more drastic compared to BZ Cam or MV Lyr. The second maximum of X-rays seem to be right before/at around when the wind strength maximizes (over the orbital phase) as the $H\alpha$ line equivalent widths maximize calculated from the blue shifted P Cygni absorption profiles. Note that for V592 Cas, both the He I $\lambda 5876$ line and the $H\alpha$ line have a single peak variation over the orbit, whereas the X-rays show double peaks within the orbit relevant to the bipolar wind nature of the source. For BZ Cam, the maximum X-ray variation is about 67% in the X-ray count rate and the X-ray variation of MV Lyr is about 50% in the count rates. For these two sources, the relative phasing between the X-rays and the optical is not definitive because the error on the orbital periods fold close to one full phase since the given time zero. For V592 Cas, error on the relative phasing between the optical and the X-rays are less than 0.05. We cannot conclusively calculate the modulation amplitudes or significance of the X-ray variations over the orbit since the data is about 15 ksec for each NL and covers only less than two cycles of the orbit at best. For MV Lyr, a complete coverage does not exist. We notice that the X-ray variations for these sources do not follow a sinusoidal shape over the orbit. Analyses of energy dependence of X-ray variations are performed using two energy bands of 0.3-2.2 keV (or 0.3-1.0 keV) and 2.5-7.0 keV revealing no significant change in the shape of the mean light curves over these energy bands, given the statistical errors of the low count rates which indicates no significant energy dependence in variations over the *Swift* XRT range.

In addition, we looked for other periodicities or coherent QPOs (quasi-periodic oscillation) that could exist in the XRT data using fast fourier transform (FFT) analysis and/or averaging several power spectra by segregating data into several smaller time intervals. We found no significant periodicity or coherent QPO for BZ Cam, V592 Cas or MV Lyr given the S/N quality of the data.

6. Spectral Analysis

A spectrum and a background spectrum was generated for each NL using all available data presented in Table 2 between 0.2-10 keV. A circular photon extraction region of radius 1.5 arc min is used for both the source and the background (devoid of other contaminating sources). Each spectrum was grouped to have a minimum of 30-60 counts in each bin to increase signal to noise and utilize good χ^2 statistics. We emphasize that the data is of moderate spectral resolution and no significant line emission other than predicted by the fitted models was detected; particularly, no iron lines at 6.4 keV, 6.7 keV or 6.9 keV was found, and so no reflection component can be confirmed with this data. However, NLs have hot disks with winds, as opposed to cold disks of quiescent DN, which may yield complicated reflection effects that may not be revealed properly with *Swift* data in the 0.2-10.0 keV band. Subsequently, these spectra are analyzed using single/double/triple thermal plasma emission models MEKAL/APEC (thermal plasma in collisional equilibrium) within XSPEC software or multi-temperature isobaric cooling flow (plasma) models CEVMKL or MKCFLOW in XSPEC (for references and model descriptions see Arnaud 1996, or <https://heasarc.gsfc.nasa.gov/xanadu/xspec/manual/Models.html>). To account for the absorption in the X-ray spectrum of interstellar or possible intrinsic origin, we utilized the *tbabs* model in the fitting procedure (Wilms, Allen & McCray 2000).

In general, the X-ray spectra of nonmagnetic CVs are well modelled with the multi-temperature isobaric cooling flow type plasma emission models as in MKCFLOW or CEVMKL (Mukai et al. 2003, Baskill et al. 2005, Pandel et al. 2005, Guver et al. 2006, Okada et al. 2008, Balman et al. 2011, Balman 2014). The X-ray spectra of nonmagnetic CVs show several different emission lines, revealing the existence of hot, optically thin plasma in these systems (see also Balman 2012). A wide range of temperatures is derived from these spectra revealed by the presence of detected H- and He-like emission lines from elements N to Fe, and some Fe L-shell lines. As the accreting material settles onto the WD through the BL region, it is expected to form a structure with continuous temperature distribution in the X-rays. This characteristic is consistent with an isobaric cooling flow plasma model which is a multi-temperature distribution of plasma with a differential emission measure assuming a power-law distribution of temperatures ($dEM = (T/T_{max})^{\alpha-1} dT/T_{max}$). In such a model, the emission measure at each temperature is proportional to the time the cooling gas remains at this temperature (Pandel et al. 2005). This type of plasma emission represent collisionally ionized plasma in thermal equilibrium between ions/protons and electrons just like the standard MEKAL/APEC models assume.

The XRT spectrum of BZ Cam was fitted using several plasma models within XSPEC. A single or double MEKAL model fits yield unacceptable χ^2_ν values of 2.6 and 2.1, respectively.

Increasing MEKAL components reduces the χ^2_ν artificially, but approximates a multiple-temperature distribution plasma. Therefore, as discussed above, a more physical model CEVMKL which is a multi-temperature plasma emission model built from the *MEKAL* code (Mewe et al. 1986) is used to fit the data. However, the data was found inconsistent with a χ^2_ν of 2.7 . BZ Cam has strong wind outflows (in the UV and optical bands) as discussed in the introduction and it may be that there is an excessive component in the X-ray spectrum due to scattering off of the wind or an emission component due to an extended structure on the disk. We used a power law model to characterize this second component and fitted the spectrum with *tbabs*×(CEVMKL+POWER) composite model. The resulting spectral parameters with an acceptable χ^2_ν are given in Table 3 (middle column) and the fitted spectrum is displayed in Figure 2. We carefully checked that all spectral parameter ranges are consistent across spectral binning of 30-60 counts per bin for the fitted model with the minimum χ^2_ν values. However, the χ^2_ν values of the unacceptable fits in this paragraph are even higher when the spectrum with 60 counts per bin is used which is expected since the greater binning increases the discrepancies between the model and data reducing statistical errors. The excess data are in the harder energy band.

For fitting the XRT spectrum of MV Lyr, we assumed similar models. A single MEKAL model fit yields an unacceptable χ^2_ν value of 2.64 . A double MEKAL model gives acceptable fits with a lower temperature of kT=0.2 keV and a higher temperature of kT=79.8 keV (a 2σ lower limit on the high temperature MEKAL model is kT=29 keV). This signals a definite distribution of temperatures where the MEKAL components somehow reflect the lower and higher temperature limits. Thus, we fitted the spectrum with a CEVMKL model alone, which yielded a χ^2_ν value of 1.7(dof.21). In order to look for any scattering effect of X-rays from a wind or a component relating to an extended structure, as in BZ Cam (note that this system is also known to have winds in the UV/optical), we added a power law component and calculated how much this composite model *tbabs*×(CEVMKL+POWER) improves the fit performed using only the CEVMKL model. The spectral parameters and the χ^2_ν value of this new/composite fit is given in Table 3 (left hand column), and the modeled spectrum is presented in Figure 3 . We tested the significance of adding the second power law component to the CEVMKL model with FTEST and found that it improves the fit at 98.6% confidence level (probab. 0.014), which is almost at 3σ significance. Note that when the binning in the spectrum is increased to a minimum of 60 counts per bin, the single CEVMKL fit has a χ^2_ν value of 2.0 which is then improved over 3σ significance when the power law model is added to the fit. The power law model removes the excess data in the harder energy band. Increasing the binning improves the S/N of the spectral bins which in turn affects the χ^2 statistics of spectral fits that do not model the spectrum adequately. This method reveals a correct spectral model that describes the spectrum, given the moderate spectral resolution

and S/N of the data.

Our final target, V592 Cas, was the lowest count rate source of the three NLs. We treated the modeling of the XRT spectrum in a similar manner as in the other two. However, in this case it is more difficult to choose between the models relying only on χ^2_ν values due to the lower statistical quality of the data. A single MEKAL model fit yields a χ^2_ν value of 1.5 with an X-ray temperature of $kT=41$ keV (a 2σ lower limit is $kT=15$ keV). Adding a second MEKAL component yields two temperatures of 0.4 keV and 8.1 keV improving the χ^2 of the fit at 92% confidence level (probab. 0.08 using FTEST). Inclusion of another MEKAL does improve the fit even more, but then it is redundant since it indicates existence of a distribution of temperatures. Thus, for the consistency of the modeling of V592 Cas with the other two NLs, we included a fit using the model *tbabs*×*CEVMKL* yielding a χ^2_ν value better than a single MEKAL fit at 94% confidence level (using FTEST). We present this fit in Table 3 (right hand column) and the fitted spectrum is shown in Figure 4. In this case, inclusion of a secondary power law component does not improve the fit (yields χ^2_ν value of 1.25). However, we include maximum limits on the power law flux and photon index for completeness. We caution that the non-detection of a significant power law component could be a result of the lower X-ray flux of the source.

The unabsorbed X-ray flux and luminosities (calculated from the distances in Table 1) of the three NL systems are given in Table 3 along with the rest of the spectral parameters with errors stated at the 90% confidence level for a single parameter. We caution that due to the energy range of *Swift* XRT and the hardness of the X-ray spectra, we may have not determined the power law photon indices as accurately and they may be in a steeper range as in 1.0-2.0 as opposed to 0.5-1.0 as seen from Table 3. Given the unabsorbed total X-ray fluxes of these sources (also, using the power law photon indices and fluxes) and the XRT count rates, *Swift* BAT is not expected to detect these sources, with an expected BAT rate $\leq 2 \times 10^{-4}$ c s $^{-1}$. We have analyzed the BAT data and have not detected any of the sources, as expected.

The range of neutral hydrogen column densities derived from the spectral fits (see Table 3), are checked using standard tools that calculate neutral hydrogen column in the line of sight: (1) COLDEN (using Dickey & Lockman 1990, <http://cxc.harvard.edu/toolkit/colden.jsp>); (2) *nhtot* (using Willingale et al. 2013, <http://www.swift.ac.uk/analysis/nhtot/index.php>). Willingale et al. (2013) calculate the molecular hydrogen column density, $N(H_2)$, in the Milky Way Galaxy using a function that depends on the product of the atomic hydrogen column density, $N(HI)$, and dust extinction, $E(B-V)$, with the aid of the 21 cm radio emission maps and the *Swift* GRB data. Using these software, we found N_H in a range, $0.6-0.7 \times 10^{21}$ cm $^{-2}$, $0.8-1.2 \times 10^{21}$ cm $^{-2}$, and $3.1-4.3 \times 10^{21}$ cm $^{-2}$ for MV Lyr, BZ Cam and V592 Cas, re-

spectively. Our N_H values are consistent with interstellar N_H within 90% confidence level errors. The fits on Table 3 are performed over a range of binning between 30-60 counts per bin, checking the soft X-ray range and the tabulated values and errors of N_H down to 0.4 keV and the hard X-ray band out to 7.5 keV.

We note that there was a preprint of a conference proceeding put in the archive (astro-ph) by Zemko & Orio (2013) including some preliminary XRT analysis of two of the sources BZ Cam and MV Lyr in our study which was after the submission of this paper to the *Astrophysical Journal*. These authors use *Raymond-Smith* and APEC models that are similar to the MEKAL models used in this study but do not use the expected multi-temperature distribution plasma models (e.g. CEVMKL, MKCFLOW) as discussed in this section.

Finally, we note that though some acceptable fits may be achieved with higher N_H (e.g. using partial covering absorbers ect.) than interstellar N_H values using the *Swift* data, such models with higher N_H do not reproduce the detected *ROSAT* count rates for these sources by factors of 3-100 times. Thus, they are not consistent with a global model for our targets in the 0.1-10 keV (or 0.1-50 keV) range.

6.1. On the existence of blackbody emission components

We do not find blackbody emission components consistent with our XRT spectra in our modeling. For completeness, we exploit the data to calculate 2σ upper limits on temperatures and fluxes for blackbody emission consistent with BL emission in which we have reduced the binning in the data and included a softer energy range down to 0.4 keV. We calculate (1) in a range of $kT_{BB}=(20-50)$ eV, an upper limit on the soft X-ray luminosity (blackbody) 6.6×10^{32} erg s $^{-1}$ for MV Lyr in the 0.1-10.0 keV band; (2) in a range of $kT_{BB}=(25-50)$ eV, a soft X-ray luminosity upper limit is 5.2×10^{32} erg s $^{-1}$ in the 0.1-10.0 keV band consistent with V592 Cas; (3) For $kT_{BB}=30$ eV upper limit, we find a soft X-ray luminosity upper limit of 2.3×10^{33} erg s $^{-1}$ in the 0.1-10.0 keV band for BZ Cam. We can not calculate upper limits on the soft X-ray flux/luminosity for effective temperatures lower than the given values/ranges in the above calculation. For larger effective temperatures than the given values/ranges, the flux/luminosity upper limits are at lower values (i.e., $\leq 1 \times 10^{32}$ erg s $^{-1}$) than these upper limits. We caution that these upper limits are not better than *ROSAT* results in the literature due to the energy band width of *Swift* and its soft sensitivity. We stress that the comprehensive *ROSAT* analysis of the 11 nonmagnetic NL systems, with its better soft X-ray sensitivity in the 0.1-2.4 keV band, demonstrates that the hardness ratios of these sources are not compatible with blackbody emission (cf. Fig 2 from van Teeseling et al. 1996) and they are consistent with optically thin plasma emission. A joint *ROSAT* and

EUVE data analysis of IX Vel (another NL) shows no blackbody emission (van Teeseling et al. 1995).

Therefore, we acquired the archival *ROSAT* data of MV Lyr (PSPCB detector), BZ Cam (PSPCB detector), and V592 Cas (PSPCC detector), and analyzed the data using the model of $tbabs \times CEVMKL$ and $tbabs \times (BBODY + CEVMKL)$ utilizing the response files *pspcc-gain1-256.rsp* and *pspcb-gain2-256.rsp*. We used observations obtained in the high states. The main goal of this analysis was to derive possible 2σ temperature upper limits for any soft blackbody emission consistent with BLs. Our fits using the CEVMKL model yielded acceptable χ^2_ν values ($\chi^2_\nu=1.0-1.2$) with parameters close to the best-fit spectral parameters and in the error ranges given in Table 3. We do not present these since the derived results are similar with the ones in Table 3. The α parameter for the power law index of the temperature distribution in CEVMKL model was fixed at the best fit values in Table 3 for BZ Cam and V592 Cas. We note that we have not included the power law spectral component in the fits since the *ROSAT* fits were conducted in 0.1-2.2 keV band, and this model will not be detected along with the thermal plasma emission component, in the narrow energy band. In order to calculate the 2σ blackbody temperature upper limits, we added a second component of BBODY (in XSPEC) in the modeling. The fits yielded the following results: (1) MV Lyr, $kT_{BB} < 6.6$ eV; (2) BZ Cam, $kT_{BB} < 5.4$ eV; and (3) V592 Cas, $kT_{BB} < 7.1$ eV. These 2σ blackbody temperature upper limits are consistent with the detected or expected WD temperatures in these NLs and not with any optically thick boundary layer emission. We note that if single MEKAL models are used for the fitting, the derived temperature upper limits are very similar.

7. Discussion

NLs have not been thoroughly investigated using the recent X-ray telescopes with higher sensitivity, wider energy band and better energy resolution in comparison with older mission studies of *ROSAT* and *EINSTEIN*. We observed a selected group of non-magnetic NLs studied only with *ROSAT* in a narrow energy band to further investigate their spectral and temporal characteristics using *Swift*. X-ray observations of BLs in NL systems are important to study characteristics under the effect of high accretion rates, to investigate the geometry of the inner disk, to calculate the BL temperature, BL luminosity, and mass accretion rate. With simultaneous X-ray and UV observations, one can work on a self-consistent model of the BL and the accretion disk.

We have presented the *Swift* XRT spectral and temporal analysis of three NL systems, MV Lyr, BZ Cam and V592 Cas. The temporal analysis indicates that all systems show

X-ray variations over the binary orbit as observed in the mean light curves. We suggest this may be related to scattering over the accretion disk. This may result from a modulated disk wind or an elevated disk rim in the accretion impact zone. However, the latter requires high inclination that is not consistent with these sources. Thus, scattering from disk winds that are episodic and modulated with the orbital period, is likely to create the X-ray variations over the orbit in accordance with the wind activity. However, it is important to note that the variations seem to follow the wind outflows as they maximize with the orbital modulation of the $H\alpha$ line which also shows P Cygni profiles (see V592 Cas). This indicates that the X-ray emitting regions may be at the base of these strong wind outflows. There is a need for better/longer X-ray time series data with simultaneous photometric light curves in the optical and UV for direct comparisons.

The *Swift* XRT spectral analysis of the three sources reveals hard X-ray emission with high X-ray temperatures in the 0.2-10.0 keV range. We found an X-ray temperature $kT_{max} > 21$ keV for MV Lyr, $33.3^{+16.0}_{-14.0}$ keV for BZ Cam and $35.5^{+19.7}_{-10.9}$ keV for V592 Cas. Among the three sources MV Lyr has the hardest X-ray spectrum, thus the maximum limit of the temperature was not constrained in the *Swift* band (see Table 3 for a best fit value). Corresponding X-ray luminosities of the thermal plasma emission are 2×10^{31} erg s $^{-1}$, 2.2×10^{31} erg s $^{-1}$ and 5.3×10^{31} erg s $^{-1}$, respectively, calculated from the CEVMKL model (i.e., fitted model) parameters. The total X-ray luminosities (thermal+power law) are 1.7×10^{32} erg s $^{-1}$ for MV Lyr, 4.6×10^{32} erg s $^{-1}$ for BZ Cam, and 5.3×10^{31} erg s $^{-1}$ for V592 Cas in the 0.2-10.0 keV energy band. We calculated that in the 0.1-50 keV band (where bulk of the X-ray emission is) the X-ray luminosities of the thermal CEVMKL components are 1.9×10^{32} erg s $^{-1}$, 5.0×10^{32} erg s $^{-1}$, and 8.5×10^{31} erg s $^{-1}$, for MV Lyr, BZ Cam, and V592 Cas, respectively. The fits for MV Lyr and BZ Cam involves a second spectral component. In order to double check the plausible under estimation of the thermal plasma emission luminosity, we assumed a single CEVMKL component fit for these two sources. We fitted the *tbabs*×CEVMKL model fixing the maximum plasma emission temperatures from the fits in Table 3, which resulted acceptable χ^2_{ν} . We re-calculated the thermal plasma emission luminosity in the 0.1-50 keV band for these sources and found 3.2×10^{32} erg s $^{-1}$, and 7.0×10^{32} erg s $^{-1}$ for MV Lyr and BZ Cam, respectively. Thus, we are not underestimating the thermal plasma luminosities from the optically thin boundary layers. The X-ray flux and luminosity of the power law components, may change considerably in the 0.1-50 keV band due to the power law index and the cut-off energy from the thermal electron distribution. Thus, it needs to be determined from fits in a larger energy band width. We note that power law components are not part of the transferred accretion power of the systems but are related to additional scatterings.

As summarized in the introduction, the X-ray emission from about 11 NLs have been

studied with *ROSAT* and found to show optically thin emission with a single MEKAL model at temperatures < 6 keV (best fit values) and luminosities $< 10^{32}$ erg s $^{-1}$. A few NLs were studied with *ASCA* and modeled with double MEKAL models at different temperatures (e.g., TT Ari and KT Aur, Mauche & Mukai 2002), and one with *XMM-Newton* using multiple-temperature plasma and MEKAL models (Pratt et al. 2004). Note that in all these observations the X-ray luminosities are \leq a few $\times 10^{32}$ erg s $^{-1}$. Greiner (1998) found blackbody model of emission more consistent with *ROSAT* spectra with (0.2-0.5) keV temperatures and hydrogen column densities of interstellar values however, with very small emitting regions. Other than these blackbody temperatures, *ROSAT* (0.1-2.4 keV) does not reveal any blackbody component in NL spectra given the suitable soft X-ray energy band and its sensitivity. In addition, the *ASCA* and *XMM-Newton* data do not reveal these hot blackbodies or any blackbody emission. Most of these results are in accordance with our findings and we find hard X-ray spectra with multi-temperature optically thin plasma emission in the *Swift* energy band without a blackbody emission, component consistent with *ROSAT* 2σ upper limits for blackbody emission with $kT < 7$ eV.

We have calculated the accretion rates in the hard X-ray emitting BLs of our systems ($L_{BL} = \dot{M} / 2R_{WD}$). The accretion rate in the boundary layer is 6.7×10^{-11} M_{\odot} yr $^{-1}$ for MV Lyr, 1.4×10^{-10} M_{\odot} yr $^{-1}$ for BZ Cam and 1.9×10^{-11} M_{\odot} yr $^{-1}$ for V592 Cas. For these calculations, values of M_{WD} and R_{WD} are assumed from Table 1 (for BZ Cam a similar WD mass and radius is taken as in MV Lyr) and thermal plasma emission luminosities in the 0.1-50 keV band have been used. It is of importance to compare our observational results with theoretical calculations of standard steady-state disk models, e.g. of Narayan & Popham (1993), and Popham & Narayan (1995). Taking the accretion rates calculated for these NLs in the optical and UV bands 1.3×10^{-8} M_{\odot} - 3.9×10^{-9} M_{\odot} (see Table 1), the standard disk models mostly predict optically thick BLs showing a blackbody emission spectrum with temperatures of 13-33 eV and $L_{soft} \geq 1 \times 10^{34}$ for an 0.8-1.0 M_{\odot} WD, (WD rotation as fast as $\Omega_* = 0.5\Omega_K(R_*)$ is taken into account in L_{soft} , see Popham & Narayan (1995)). We underline that this blackbody temperature range is definitely larger than the 2σ upper limits we derive from the *ROSAT* data and the luminosity range seems larger than the luminosity range (0.1-10.0 keV) we calculated from the *Swift* data (see section 6.1). The standard steady-state constant \dot{M} disk models predict (for optically thin emission) X-ray temperatures around 9-10 keV for a 1 M_{\odot} WD at about 3.2×10^{-10} M_{\odot} (see Narayan & Popham 1993).

Comparing the accretion disk luminosity from Table 1 and the X-ray luminosity of the thermal plasma emission from these three NLs, (1.8×10^{32} erg s $^{-1}$, 5.0×10^{32} erg s $^{-1}$ and 8.5×10^{31} erg s $^{-1}$, for MV Lyr, BZ Cam, and V592 Cas, respectively) we find that the ratio $L_x / L_{disk} \sim 0.01$ -0.001. The accretion rates and luminosities calculated using the X-ray

data of these NLs resemble dwarf novae in quiescence. However, the optical and UV rates and luminosities for NL disks in the same brightness states resemble those of dwarf novae in outburst. For nonmagnetic systems, the earlier studies of the ratio of the X-ray flux to optical and/or UV flux, F_x/F_{opt} , decreased along the sequence SU UMa stars ($F_x/F_{opt} \sim 0.1$)- U Gem stars- Z Cam stars ($F_x/F_{opt} \sim 0.01$) - UX UMa stars and high state VY Scl stars ($F_x/F_{opt} \leq 0.001$) using the *EINSTEIN* and *ROSAT* results (see Kuulkers et al. 2006, van Teeseling et al. 1996, Patterson & Raymond 1985). This ratio is found to decrease with increasing P_{orb} and increasing \dot{M} where a high \dot{M} causes the disk to emit more UV flux, but not as much X-ray flux (see review by Kuulkers et al. 2006).

The virial temperature in the inner parts of the accretion disk ($kT_{virial} = \mu m_p GM_{WD}/3R_{WD}$ where $\mu \sim 0.6$ and m_p is the proton mass) limits the maximum plasma emission temperatures in nonmagnetic CVs (see also Pandel et al. 2005 for dwarf novae in quiescence). All the kinetic energy from the Keplerian motion of the accreting gas is converted into heat when virial temperatures are acquired by the flow. This gives the maximum energy per particle that can be dissipated and the temperature of standard 1-D boundary layers cannot be around the virial temperatures or material can not be confined to the disk. Given the WD properties on Table 2, if one assumes similar properties for the three NLs in question, we calculate $T_{virial} = 27$ keV for these NLs. Energy budget of a radiative isobaric cooling flow indicates that T_{max} is smaller than T_{virial} . The cooling flow releases an energy of $(5/2)kT_{max}$ per particle including kinetic and compressional components. The total thermal/kinetic energy at the inner edge of the disk available per particle is $(3/2)kT_{virial}$. This in turn yields another constraint that $T_{max}/T_{virial} < 3/5$. Therefore, given $T_{virial} = 27$ keV, then $T_{max} \leq 16$ keV. All of the best fit X-ray temperatures are above the calculated virial temperature and T_{max} constraint. We also calculated the 2σ lower limits of the X-ray temperatures to compare with our T_{virial} and T_{max} estimations and find that for BZ Cam the limit is > 17 keV and for MV Lyr and BZ Cam, it is > 21 keV. As a result, the boundary layers in these NLs are too hot, thus may not be confined to the disk and will expand/evaporate forming **ADAF-like flows/X-ray coronal regions** where the accreting material will be advected onto the WD. We stress that all the multi-temperature plasma model fits show that the α parameter in these fits differ from 1.0 and that the cooling flows are non-standard as well revealing a different type of flow.

ADAFs (Advection-dominated flows) correspond to a condition where the gas is radiatively inefficient and the accretion flow is underluminous (see Narayan & McClintock 2008, Lasota 2008, Done et al. 2007). Advection-dominated accretion may be described in two different regimes. The first is when the accreting material has a very low density and a long cooling time (also referred as RIAF-radiatively inefficient accretion flow) with $t_{cool} > t_{acc}$ (t_{cool} is the cooling time and t_{acc} is the accretion time). This causes the accretion

flow temperatures to be virialized in the ADAF region. Note that the standard ADAFs are two-temperature flows as studied in LMXBs where electrons and ions are at differing temperatures. The electron temperatures increase with decreasing accretion rate. For example, Atoll type relatively low accretion rate (compared to Z-sources) neutron star LMXBs (type-I bursters) show 1-200 keV spectra consistent with thermal Comptonization with a plasma electron temperature around 25-30 keV and some are found at even lower X-ray temperatures (see Barret et al. 2000 and Done et al. 2007). These systems show an optically thin BL as the main region of energy release merged with an ADAF. These sources have similar accretion rates to NLs if the ratio to \dot{M}_{Edd} is considered in relative terms. Note that neutron stars in Atoll sources should be accreting substantial material as revealed in their X-ray bursts. For LMXBs hosting black holes the ADAFs have detected temperatures about 100 keV. For CVs virial temperatures in the disk are around 10-45 keV where the WDs are primaries as opposed to neutron stars or black holes (assuming $0.4 M_{\odot}$ - $1.1 M_{\odot}$ WDs).

The second regime is such that the particles in the gas can cool effectively, but the scattering optical depth of the accreting material is large enough that the radiation can not escape from the system (see also "slim disk" model Abramowicz et al. 1988). The defining condition is then, $t_{\text{diff}} > t_{\text{acc}}$ (t_{diff} is the diffusion time for photons). This regime requires high accretion rates of the order of $0.1\dot{M}_{\text{Edd}}$. We stress that the mass accretion rates derived from the optical and UV observations for the three NLs in this paper are below this critical limit for a slim disk approach.

In an RIAF-ADAF region (first regime) energy liberated by viscous dissipation remains in the gas and the energy is advected onto the compact star given some ratio of advection energy and viscous dissipation. Thus, the pressure and hence the sound speed are large. The accretion flow becomes geometrically thick, with high pressure support in the radial direction which causes the angular velocity to stay at sub-Keplerian values, and the radial velocity of the gas becomes relatively large with $\alpha \sim 0.1-0.3$. This leads to a short accretion time $t_{\text{acc}} \sim R/v \sim t_{\text{ff}}/\alpha$ (t_{ff} : free fall timescale; see Narayan & McClintock 2008). Finally, the gas with the large velocity and scale height will have low density, since the cooling time is long, and the medium will be optically thin.

It is widely accepted that there is strong connection/association between ADAFs and outflows as in winds and jets/collimated outflows (see Narayan & Yi 1995, Blandford & Begelman 1999). This is largely because the ADAFs have positive Bernoulli parameter defined as the sum of the kinetic energy, potential energy and enthalpy, thus the gas is not well bound to the central star. We point out that a lot of the NL systems have strong wind outflows and particularly, two of the NLs studied in this paper, BZ Cam and V592 Cas, have strong bipolar collimated wind outflows modulated with the orbital period (e.g.,

rotates obliquely to the observer’s line of sight), as detected in the optical and UV bands with high velocities 3000-5000 km s⁻¹ (see Introduction). Given these characteristics, we suggest that the ADAF-like optically thin BLs may be the origin of these wind outflows from these systems. Mass loss rates of winds in NLs are about or less than 1% of the accretion rate, with acceleration length scale of about (20-100) R_{WD} which are strongly affected by rotation (Kafka & Honeycutt 2004, Long & Knigge 2002). For V592 Cas, as noted earlier in the Introduction, optical brightness variations are not correlated with the strength of the wind outflows, and the outflow shows orbital variations and no variations relating to a disk tilt, disk precession or any superhump period of the system. Moreover, in the UV emitting inner disk, Froning et al. (2012) finds that the continuum does not vary in a good fraction of the target NLs, revealing that changes in the wind structure are not tied to the accretion disk. These are a few hints that the origin of the wind outflow may be in the ADAF-like BL, not the disk itself. We note that BZ Cam is a CV embedded in a nebula not related to a nova explosion. It has been suggested that interactions of the BZ Cam wind with the interstellar medium produces the observed nebular bow shock (Hollis et al. 1992), but alternative origins for the nebula have also been proposed (e.g., Griffith et al. 1995; Greiner et al. 2001).

Narayan & Popham (1993) show that the optically thin BLs of accreting WDs in CVs can be radially extended and that they advect part of the viscously dissipated energy as a result of their inability to cool, therefore indicating that optically thin BLs act as ADAF-like accretion flows. Partial radial pressure support by the hot gas also results in sub-Keplerian rotation profiles in these solutions. Advection can play an important role for the energy budget and the emission spectrum of the accretion flow in the BL. In addition, Popham & Narayan (1995) illustrate that the BL can stay optically thin even at high accretion rates for optical depth $\tau < 1$ together with $\alpha > 0.1$. However, such models are not well investigated. For simplicity an ADAF around a WD can be described by truncating the ADAF solutions (as opposed to BHs) and the accretion energy is advected onto the WD heating it up. Accretion via a standard disk boundary layer is expected to spin-up a WD except when rotating near breakup (Popham & Narayan 1991), however a WD is spun down when accreting via ADAF-like hot flows (Medvedev & Menou 2002). Sion (1999) emphasizes that rapidly rotating WDs are rare in nonmagnetic CVs. For some preliminary modeling of ADAFs or hot settling flows (for CVs) see Medvedev & Menou (2002) and related references therein. The ADAF models in CVs should utilize reemission of the energy advected by the flow, modeled as a single-temperature blackbody of temperature: $T_{eff} = (L_{adv}/4f\pi\sigma R_{wd}^2)^{1/4}$ where f is the fraction of the stellar surface that is emitting. In addition, we note that Godon & Sion (2003) have calculated that WDs in DN are not generally heated to more than 15% above their original temperature via standard steady-state disk accretion, even through multiple DN outbursts. Hence, other mechanisms are necessary (e.g. compressional heating, heating via advective

accretion flows, irradiation via luminous optically thick boundary layer). Characteristics of ADAF-like flows may be different in CVs, since WDs are less compact than stellar-mass BHs, the hot flows will have less extend around a WD. Menou (2000) suggests that the gas in the hot flow is one-temperature (1-T implying plasma in collisional ionization equilibrium–CIE), because of the efficient Coulomb interactions at lower temperatures compared to BHs and that the energy advection is not dependent on the preferential heating of the ions by the viscous dissipation and lack of energy exchange between the ions and the electrons necessary for the two-temperature ADAFs in BH binaries (2-T implying a type of non-equilibrium ionization plasma–NEI). We note here that since there are no detailed theoretical calculations for ADAF flows in CVs, existence of 2-T ADAFs for CVs can not be completely ruled out which may yield a rather featureless X-ray spectra. The energy advected by the flow is lost through the event horizon in the BHs whereas in the CVs, it is expected to be re-radiated from the surface of the WD. The resulting EUV emission (and/or hard X-ray emission from the BL) could explain the strength of HeII $\lambda 4686$ emission line as due to disk irradiation.

One can compare the WD temperatures/heating in magnetic CVs (MCVs) and NL systems. This is only to calculate an approximate radiation efficiency for the BLs in NLs since MCVs particularly Polars, have different accretion geometry (they do not have accretion disk) and thus, does not accrete through advective hot flows. MCVs are known to have radiative shocks in accretion columns over the magnetic polar caps heating the WDs through basically radiative accretion flows. The Polar subtypes have been found to host cooler WDs compared with nonmagnetic CVs at the same orbital period (Sion 1999, Araujo-Betancor et al. 2005, Townsley & Gansicke 2009). The accreted material in these systems (possibly valid for IPs) are constrained by the magnetic field to the polar regions down to a limited pressure depth. Strong lateral pressure gradients forces this material to spread over the surface. As a result, heat dissipated by compression up to a critical pressure is constrained to the polar regions, and compression at further higher pressures is spread over the whole surface heating the WD (Townsley & Gansicke 2009). The average WD temperature is about 50,000 K and about 16,000 K in NLs and MCVs (Polars), respectively above the period gap between 3-5 hrs (see Townsley & Gansicke 2009, Mizusawa et al. 2010). The relative luminosity difference of the WDs as a result of these temperatures is $L_{adv}/L_{rad} = (50000/16000)^4$ (assuming similar R_{WD}). This ratio is about 96 which means that about 96 times more accretion power may be transferred to the WD in NLs. This will approximately result in about a factor of 96 times reduction in the radiation power from the BL since this power is advected onto the WD yielding a radiation inefficiency in the BL of about 0.01; we may denote this as ϵ_{adv} . We note that if one assumes average temperature from the total samples of Polars and NLs, $L_{adv}/L_{rad} = (45000/13500)^4 = 123$, yielding an approximate $\epsilon_{adv} \sim 0.008$ (same average R_{WD} assumed).

As we have discussed in the previous paragraphs it has been proposed that ADAFs can have thermally-driven winds (Narayan & Yi 1995, Blandford & Begelman 1999) possibly modified/controlled by magnetic fields that would carry away some of the accretion power in the BL which is, then, not radiated by the BL. This does not necessarily imply that all NL winds are to originate from the BL. Therefore, the power/energy necessary to derive the wind outflows from BLs will also yield inefficiency in the radiation from the BL in the NLs ; we may denote this as ϵ_{wind} . The wind luminosity, which represents the kinetic energy loss of the wind, is described as $L_{wind}=(\dot{M}_{wind}v_{\infty}^2)/2$. Not all the power used to derive the wind outflows appears as the kinetic power of the outflow and there is a certain efficiency factor associated with this conversion that changes from typically 10^{-1} - 10^{-4} for stellar winds (Lamers & Cassinelli 1999) or 10^{-3} - 10^{-4} for AGNs (Yuan & Narayan 2014). Assuming 1% of the power used to drive the wind outflows appears as the kinetic power of the outflow defined as the wind luminosity, $L_{outflow-BL}=L_{wind}/0.01$. Using a wind speed of 3000 km s^{-1} and a mass loss rate of $1 \times 10^{-10} \text{ M}_{\odot} \text{ yr}^{-1}$ (Kafka et al. 2009), L_{wind} is $3 \times 10^{32} \text{ erg s}^{-1}$ which will reduce the BL radiation by about $3 \times 10^{34} \text{ erg s}^{-1}$ in V592 Cas. The same calculation using 5000 km s^{-1} and $1 \times 10^{-11} \text{ M}_{\odot} \text{ yr}^{-1}$ (Honeycutt et al. 2013) yields a reduction in the BL radiation by about $8 \times 10^{33} \text{ erg s}^{-1}$ in BZ Cam. The wind in MV Lyr is not as fast (see Linnell et al 2005) and does not yield strong reduction ($\leq 2 \times 10^{31} \text{ erg s}^{-1}$). Narayan & Yi (1995) predict that diminished winds/outflows may possibly occur when a hot (disk) corona forms (as viewed in the X-rays) with less effective advection-dominated flows. Overall, the efficiency of the BL radiation will be reduced by $\epsilon_{total}=\epsilon_{adv} \times \epsilon_{wind}$.

It is possible that the soft X-ray to EUV emission from the region of the BL and/or the inner disk of a steady-state disk can be screened by the existing ADAF-like/X-ray coronal region and the soft radiation from the disk can be Compton-upscattered. Another possibility is that hard X-ray photons from the BL can Compton/scatter from the existing (strong) winds in these systems. Some of these winds are axisymmetric/bipolar in nature which may lead to non-isotropic scattering. Thus, the power law components derived from our fits are crucial and signals the existence of Comptonized or Compton up-scattered radiation in these systems as described above. It may be possible that both type of thermal Comptonization or scattering is occurring in these systems. We find power law luminosities of $(0.2\text{-}2.4) \times 10^{32} \text{ erg s}^{-1}$ (consistent with only some percent of the total X-ray luminosities of these NLs). We caution that the power law components also do not account for the disk luminosity of these systems (they are about 1-0.1% of the disk luminosity).

There has been no definitive evidence that NLs are magnetic CVs; a few were suggested as intermediate polars (IP) (see Froning et al. (2012)), but have never been confirmed in X-rays. The UV and optical spectra of NLs are different from those of IPs. In particular, episodic bipolar strong wind production is not seen in the magnetic systems. The WDs in

NL systems are very hot, 2-4 times hotter (see Townsley & Gansicke 2009, Mizusawa et al. 2010 and see also Table 1) in general compared with magnetic CVs revealing differences in the accretion physics, heating and geometry. The X-ray emission in IPs show virialized hot plasma from stand-off radiative shocks in small regions (accretion column) around the magnetic poles with temperatures 10-95 keV at 10^{31-34} erg s⁻¹ (Balman 2012 and references therein). On the other hand, the most important signature of IPs is the spin period of the WDs that manifests itself in the X-ray light curves regardless of the inclination of the systems. None of our systems (and most other NLs) have detected spin periods in the X-rays and we did not detect any (see Mukai 2011 for a catalog of IPs ¹). IP X-ray spectra show complex absorption phenomenon with partial covering absorption or warm absorbers showing energy dependent modulations where we only found interstellar absorption and no energy dependence of orbital variations atypical of IPs. Moreover, IPs with high accretion rates, as detected from the optical and UV bands of these NLs may be expected to show a component with a 40-120 eV blackbody temperature resulting from reprocessing of the X-rays, for which we find no evidence. About 30% of IPs indicate this soft component (Bernardini et al. 2012). In addition, IPs do not show major high and low states as in two of our NLs. Thus, there is no consistency with a magnetic CV picture for our targets.

8. Conclusions

Observations of CV disk systems at low mass accretion rate (namely dwarf nova CVs in quiescence) have yielded the temperature and luminosity of the BLs from X-ray observations while the UV observations helped to determine the temperature and luminosity of the accreting white dwarfs, as they are the dominant component at low \dot{M} . The quiescent X-ray spectra are well characterised with a multi-temperature isobaric cooling flow model of plasma emission at $kT_{max}=6-55$ keV with accretion rates of $10^{-12}-10^{-10}$ M_⊙ yr⁻¹ and the detected Doppler broadening in lines during quiescence is <750 km s⁻¹ at mostly sub-Keplerian velocities with electron densities $>10^{12}$ cm⁻³. To further our understanding of the boundary layers in CVs and their spectral and temporal characteristics in the X-rays, we used a group of non-magnetic NLs (VY Scl and UX UMa sub-type systems) where NLs are mostly found in a state of high mass accretion rate with $\geq 1 \times 10^{-9}$ M_⊙ yr⁻¹ and some showing occasional low states (VY Scls). X-ray observations of BLs in NL systems are important to derive parameters such as the BL temperature, BL luminosity, mass accretion rate and study accretion geometry. Using both X-ray and UV observations one can then build a self-consistent model of the BL and the accretion disk.

¹ <http://asd.gsfc.nasa.gov/Koji.Mukai/iphome/catalog/alpha.html>

In this work, we presented *Swift* XRT observations of three non-magnetic NLs, MV Lyr (VY Scl type), BZ Cam (VY Scl type), and V592 Cas (UX UMa type), obtained in their high states. We find that these sources have X-ray spectra consistent with multi-temperature hot plasma emission that has a power law dependence in emission measure (i.e. temperature) distribution in a range $kT_{max}=(21-50)$ keV. We calculate that the X-ray emitting plasma is virialized. The power-law index of the temperature distribution indicates that these plasmas depart from the predictions of isobaric cooling flow type models as opposed to low \dot{M} systems like quiescent DN. We detect a second component in the X-ray spectra that is well modeled by a power law emission in the VY Scl type sources BZ Cam and MV Lyr. V592 Cas may be fitted with an additional power law model, but the fit is not significantly different than a fit without it. We do not find any periodicity in the *Swift* XRT data for the three sources, but we find non-sinusoidal variation of X-ray emission over the orbital cycle of the systems without energy dependence in the 0.2-10.0 keV band. Particularly, the mean light curve of V592 Cas indicates two separated peaks that may be associated with a bipolar outflow structure. The ratio of the unabsorbed X-ray flux/luminosity of the three systems and the disk luminosities as calculated from UV and optical wavelengths is $\sim 0.01-0.001$ where BZ Cam and MV Lyr are in the upper end and V592 Cas is in the lower end of this range indicating inefficiency of X-ray/BL radiation (note that we quote a lower limit for the disk luminosity of BZ Cam in Table 3). We do not find a blackbody emission component in the soft X-rays using our *Swift* data and also the *ROSAT* data with a 2σ upper limit of $kT_{BB} < 7$ eV for the three systems, consistent with the WD temperatures but not with the optically thick boundary layer emission.

As a result, we suggest that the BLs in NL systems may be optically thin hard X-ray emitting regions merged with ADAF-like flows and/or constitute X-ray corona regions on the inner disk close to the WD. We estimate that the high WD temperatures in the three NLs and others (NLs) may explain the efficiency reduction ϵ_{adv} in the optically thin BLs with a factor ~ 0.01 . ADAF-like accretion flows in the BLs may help to explain the very fast collimated outflows from the NL systems because ADAFs have positive Bernoulli parameter (the sum of the kinetic energy, potential energy and enthalpy). Thus, the power lost to drive a wind from the ADAF-like BLs may result in even larger losses from the accretion power in these X-ray emitting BL regions. In addition, we note that analysis in the optical and the UV wavelengths (in the IR for some) indicate departure from the standard disk model for MV Lyr (Linnell et al. 2005), BZ Cam (Godon et al. 2014, in preparation), and V592 Cas (Hoard et al. 2009). We caution that our findings in the X-rays may not be optimally analogous to the case of LMXBs thus, ADAF-like flows (1-T in CIE or plausibly 2-T in NEI) and formation of X-ray coronal regions in the BLs and/or the disk needs to be modeled for CVs in detail. We can not confirm at this stage that all NL systems have the type of

BL/inner disk structure described for these three sources in this paper.

acknowledgment

The authors thank J. P. Lasota, J. Greiner and M. Revnivtsev for careful comments on the manuscript. PG is thankful to William Patrick Blair at the Henry Augustus Rowland Department of Physics and Astronomy at the Johns Hopkins University (Baltimore, MD), for his kind hospitality. This work was supported by the National Aeronautics and Space Administration (NASA) Under grant number NNX13AJ70G issued through the Astrophysics Division Office (SWIFT Cycle 8 Guest Investigator Program) to Villanova University.

REFERENCES

- Araujo-Betancor, S. et al. 2005, *ApJ*, 622, 889
- Arnaud, K. A. 1996, *Astronomical Data Analysis Software and Systems V* (ASP Conf. Ser. 101), ed. G. H. Jacoby & J. Barnes (San Francisco, CA: ASP), 17
- Abramowicz, M. A., Czerny, B., Lasota, J. P., & Szuszkiewicz, E. 1988, *ApJ*, 332, 646
- Ballouz, R.L., & Sion, E. M. 2009, *ApJ*, 697, 1717
- Balman, S., Godon, P., Sion, E.M., Ness, J.-U., Schlegel, E., Barrett, P.E., & Szkody, P. 2011, *ApJ*, 741, 84
- Balman, S., & Revnivtsev, M. 2012, *A&A*, 546, 112
- Balman, S. 2012, *MmSAI*, 83, 585
- Balman, S. 2014, pre-print, (2014arXiv1403.4437B)
- Barret, D., Olive, J. F., Boirin, L., Done, C., Skinner, G. K., & Grindlay, J. E. 2000, *ApJ*, 533, 329
- Barthelmy, S., et al. 2004, *Proc. SPIE*, 5165, 175
- Baskill, D. S., Wheatley, P. J., & Osborne, J., P. 2005, *MNRAS*, 357, 626
- Bernardini, F., de Martino, D., Falanga, M., Mukai, K., Matt, G., Bonnet-Bidaud, J.-M., Masetti, N., & Mouchet, M. 2012, *A&A*, 542, 22

- Blandford, R. D., & Begelman, M. C. 1999, MNRAS, 303, 1
- Bruch, A., & Engel, A. 1994, A&AS, 104, 79
- Burrows, D. N., et al. 2005a, Space Sci. Rev., 120, 165
- Cardelli, J.A., Clayton, G.C., Mathis, J.S. 1989, ApJ, 345, 245
- Lamers, H.J.L., & Cassinelli, J. P. 1999, Introduction to Stellar Winds, (Cambridge: Cambridge University Press)
- Chiappetti, L., Maraschi, L., Treves, A., & Tanzi, E.G. 1982, ApJ, 258, 236
- Dickey, J. M., & Lockman, F. J. 1990, ARA&A, 28, 215
- Done, C., Gierlinski, M., & Kubota, A. 2007, A&ARv, 15, 1
- Ellis, G.L., Grayson, E.T., Bond, H.E., 1984, PASP, 96, 283
- Froning, C., Long, K.S., Gänsicke, B.T., Szkody, P. 2012, ApJS, 199, 7
- Garnavitch, P., Szkody, P. 1988, PASP, 100, 1522
- Gehrels, N., et al. 2004, ApJ, 611, 1005
- Godon, P., Regev, O., & Shaviv, G., 1995, MNRAS, 275, 1093
- Godon, P., & Sion, E.M. 2011, PASP, 123, 903
- Godon, P., Sion, E.M., Levay, K., Linnell, A.P., Szkody, P., Barrett, P.E., Hubeny, I., Blair, W.P. 2012, ApJS, 203, 29
- Godon, P. et al. 2014, (inpreparation)
- Greiner, J. 1998, A&A, 336, 626
- Greiner, J. et al. 2001, A&A, 376, 1031
- Griffith, D., Fabian, D., Sion, E.M. 1995, PASP, 107, 856
- Guinan, E.F., & Sion, E.M. 1982, ApJ, 258, 217
- Guver, T., Uluayaz, C., Ozkan, M. T., Gogus, E. 2006, MNRAS, 372, 450
- Hertfelder, M., Kley, W., Suleimanov, V., & Werner, K. 2013, A&A, 560, 56

- Hoard, D.W., Linnell, A.P., Szkody, P., Fried, R.E., Sion, E.M., Hubeny, I., & Wolfe, M.A. 2004, *ApJ*, 604, 346
- Hoard, D.W., et al. 2009, *ApJ*, 693, 236
- Hollis, J.M., Oliverson, R.J., Wagner, R.M., & Feibelman, W.A. 1992, *ApJ*, 393, 217
- Honeycutt, R.K., Kafka, S., & Robertson, J.W. 2013, *AJ*, 145, 45
- Huber, M.E., Howell, S.B., Ciardi, D.R., Fried, R. 1998, *PASP*, 110, 784
- Inogamov, N.A., & Sunyaev, R.A., 1999, *Astron. Lett.*, 25, 5
- Ishida, M., Okada, S., Hayashi, T., Nakamura, R., Terada, Y., Mukai, K., & Hamaguchi, K. 2009, *PASJ*, 61, 771
- Kafka, S., & Honeycutt, R. K. 2004, *AJ*, 128, 2420
- Kafka, S., Hoard, D. W., Honeycutt, R. K., & Deliyannis, C. P. 2009, *AJ*, 137, 197
- Kato T., 2002, *A&A*, 384, 206
- Kluźniak, 1987, PhD Thesis, Stanford University
- Long, K. & Knigge, C. 2002, *ApJ*, 579, 725
- Krautter, J., Klaas, U., & Radons, G. 1987, *A&A*, 181, 373
- Kuulkers, E., Norton, A., Schwope, A., & Warner, B. 2006, in *Compact stellar X-ray sources*, W. Lewin & M. van der Klis (ed.), Cambridge Astrophysics Series No. 39 (Cambridge, UK: Cambridge University Press), 421
- Lasota, J. P. 2008, *NewAR*, 51, 752
- la Dous, C. 1991, *A&A*, 252, 100
- Linnell, A.P., Szkody, P., Gänsicke, B.T., Long, K.S., Sion, E.M., Hoard, D.W., & Hubeny, I. 2005, *ApJ*, 624, 923
- Linnell, A.P., Godon, P., Hubeny, I., Sion, E.M., & Szkody, P. 2008, *ApJ*, 687, 568
- Lu, W., Hutchings, J.B. 1985, *PASP*, 97, 990
- Lynden-Bell, D., & Pringle, J.E. 1974, *MNRAS*, 168, 303
- Mauche, C. W. & Mukai, K. 2002, *ApJ*, 566, 33

- Medvedev, M. V., & Menou, K. 2002, *ApJ* 565, 39
- Menou, K. 2000, pre-print, (astro-ph/000785)
- Mewe, R., Lemen, J.R., van den Oord, & G.H.J. 1986, *A&AS*, 65, 511
- Mizusawa, T. et al. 2010, *PASP*, 122, 299
- Mukai, K., Kinkhabwala, A., Peterson, J. R., Kahn, S. M., & Paerels, F. 2003, *ApJ*, 586, 77
- Mukai, K.; Patterson, J. 2004, *RMxAC*, 20, 244
- Mukai, K.; Zietsman, E.; Still, M., 2009, *ApJ*, 707, 652
- Mukai, K. 2011, <http://asd.gsfc.nasa.gov/Koji.Mukai/iphone/catalog/alpha.html>
- Miyamoto, S., Kimura, K., Kitamoto, S., Dotani, T., & Ebisawa, K. 1991, *ApJ*, 383, 784
- Narayan, R., & Popham, R. 1993, *Nature*, 362, 820
- Narayan, R., & Yi, I. 1995, *ApJ*, 444, 231
- Narayan, R., & McClintock, J. E. 2008, *NewAR*, 51, 733
- Okada, S., Nakamura, R., & Ishida, M. 2008, *ApJ*, 680, 695
- Pajdosz, G., Zoha, S. 1992, in Kondo Y., Sistero R., Polidan R.S. eds., *Proc. IAU SYmp.* 151, *Evolutionary Processes in Interacting Binary Stars*, Kluwer, Dordrecht, p.441
- Pandel, D., Córdova, F.A.C.D., Mason, K.O., Priedhorsky, W.C. 2005, *ApJ*, 626, 396
- Patterson, J., Raymond, J. C., 1985, *ApJ*, 292, 535
- Patterson, J., Patino, R., Thorstensen, J.R., Harvey, D., Skillman, D.R., Ringwald, F.A. 1996, *AJ*, 111, 2422
- Patterson, J. et al. 2013, *MNRAS*, 434, 1902
- Piro, A.L., & Bildsten, L. 2004, *ApJ*, 610, 977
- Pratt, G. W., Mukai, K., Hassall, B. J. M., Naylor, T., & Wood, J. H. 2004, *MNRAS*, 348, 49
- Popham, R. 1999, *MNRAS*, 308, 979
- Popham, R., & Narayan, R., 1995, *ApJ*, 442, 337

- Popham, R., & Narayan, R., 1991, ApJ, 370, 604
- Pringle, J.E., 1977, MNRAS, 178, 195
- Pringle, J.E., 1981, ARAA, 19, 137
- Pringle, J.E., & Savonije, G., 1979, MNRAS, 197, 777
- Prinja, R.K., Ringwald, F.A., Wade, R.A., Knigge, C. 2000, MNRAS, 312, 316
- Prinja, R.K., Knigge, C., Whiterick, D.K., Long, K.S., Brammer G. 2004, MNRAS, 355, 137
- Puebla, R.E., Diaz, M.P., Hubney, I. 2007, AJ, 134, 1923
- Rana, V. R., Singh, K. P., Schlegel, E. M., & Barrett, P. E 2006, ApJ, 642, 1042
- Ringwald, F.A., & Naylor, T. 1998, AJ, 115, 286
- Ritter, H., & Kolb, U. 1998, A&AS, 129, 83
- Rodriguez-Gil, P., et al. 2007, MNRAS, 377, 174
- Roming, P. W. A., et al. 2005, Space Sci. Rev., 120, 95
- Schlegel, E.M., & Singh, J. 1995, MNRAS, 276, 1365
- Schneider, D.P., Young, P., & Shectman, S.A. 1981, ApJ, 245, 644
- Shakura, N.I., & Sunyaev, R.A. 1973, A&A, 24, 337
- Sion, E.M. 1985, ApJ, 292, 601
- Sion, E.M. 1999, PASP, 111, 759
- Skillman, D.R., Patterson, J., & Thorstensen, J.R. 1995, PASP, 107, 545
- Szkody, P., & Downes, R.A. 1982, PASP, 94, 328
- Szkody, P., Nishikida, K., Raymond, J. C., Seth, A., Hoard, D. W., Long, K. S., & Sion, E. M. 2002, ApJ, 574, 942
- Taylor, C.J., et al. 1998, PASP, 110 1148
- Thorstensen, J.R., Thomas, G., Patterson, J., paper presented at Interacting Binary Stars Conference, Meeting of the Astronomical Soc. of the Pacific, San Diego, CA, July 1993

- van Teeseling, A., Drake, J. J., Drew, J. E., Hoare, M. G., & Verbunt, F. 1995, *A&A*, 300, 808
- van Teeseling, A., Beuermann, K., Verbunt, F. 1996, *A&A*, 315, 467
- Townsley, D. M., & Gansicke, B. T. 2009, *ApJ*, 693, 1007
- Voges, W. et al. 1999, *A&A*, 349, 389
- Warner, B. 1995, *Cataclysmic Variable Stars*, (Cambridge: Cambridge University Press)
- Welsh, W. F., Skidmore, W., Wood, J. H., Cheng, F. H., & Sion, E. M. 1997, *MNRAS*, 291, 57
- Willingale, R., Starling, R. L. C., Beardmore, A. P., Tanvir, N. R., & O’Brien, P. T. 2013 *MNRAS*, 431, 394
- Wilms, J., Allen, A., & McCray, R. 2000, *ApJ*, 542, 914
- Woods, J.A., Drew, J.E., Verbunt, F. 1990, *MNRAS*, 245, 323
- Woods, J.A., Verbunt, F., Cameron, A.C., Drew, J.E., & Piers, A. 1992, *MNRAS*, 255, 237
- Wood, M.A. 1995, *LNP Vol.443: White Dwarfs*, 41
- Yuan, F., & Narayan, R. 2014, pre-print, (2014arXiv1401.0586Y)
- Zemko, P., & Orio, M. 2013, pre-print, (2013arXiv1312.5122Z)

Table 1. System Parameters

Parameter	units	MV Lyr	BZ Cam	V592 Cas
M_{wd}	M_{\odot}	0.73-0.8 ^(1,2)		0.75 ⁽¹¹⁾
R_{wd}	km	7,440 ⁽³⁾		7,378 ⁽¹¹⁾
M_{2nd}	M_{\odot}	0.3 ⁽²⁾		0.21 ⁽¹¹⁾
i	deg	10 \pm 3 ^(4,5,6)	12-40 ^(13,14)	28 \pm 10 ⁽¹⁰⁾
P	hr	3.19 ⁽⁵⁾	3.69 ^(9,17,18)	2.76 ⁽⁸⁾
d	pc	505 \pm 30 ^(1,2)	830 \pm 160 ⁽¹³⁾	330 ⁽¹⁰⁾ -360 ⁽¹¹⁾
T_{wd}	K	44,000 \pm 3000 ^(1,2)		45,000 ⁽¹¹⁾
\dot{M}_{high}	M_{\odot}/yr	3×10^{-9} ^(1,6)	$\geq 3 \times 10^{-9}$ ⁽¹⁸⁾	$\sim 1.3 \times 10^{-8}$ ⁽¹¹⁾
V	min-max	17.7-12.1	14.3-12.5	12.9-12.5
L_{disk}	$erg\ s^{-1}$	$\sim 2.7 \times 10^{34}$	$\geq 3 \times 10^{34}$	$\sim 1.2 \times 10^{35}$
Ω_*	Ω_K	~ 0.28 ⁽¹⁾		

References: (1) Godon et al. (2012); (2) Hoard et al. (2004); (3) Wood (1995); (4) Schneider et al. (1981); (5) Skillman et al. (1995); (6) Linnell et al. (2005); (7) Bruch & Engel (1994); (8) Taylor et al. (1998); (9) Patterson et al. (1996); (10) Huber et al. (1998); (11) Hoard et al. (2009); (12) Cardelli et al. (1989); (13) Ringwald & Naylor (1998); (14) la Dous (1991); (16) Prinja et al. (2000); (17) Honeycutt et al. (2013); (18) Thorstensen et al. (1993); (19) Ballouz & Sion (2009).

Table 2. *SWIFT* Observation Log

System Name	Obs ID	Seg	Date (UT) yyyy-mm-dd	Time (UT) hh:mm:ss	Exp. Time seconds	UVOT mode	XRT mode
MV Lyr	91443	4	2012-06-09	09:19:01	6600.00	0x122f	PC/WT
MV Lyr	91443	2	2012-06-08	09:04:01	7640.00	0x122f	PC/WT
BZ Cam	91441	2	2012-12-21	10:05:59	1240.00	0x122f	PC/WT
BZ Cam	91441	2	2012-12-21	10:09:59	13860.00	0x122f	PC/WT
V592 Cas	91442	4	2012-09-10	09:49:59	6865.00	0x122f	PC/WT
V592 Cas	91442	2	2012-09-09	04:44:45	6385.00	0x122f	PC/WT

Table 3. Spectral Parameters of the Fits to the NL Spectra

Model	Parameter	MV Lyr	BZ Cam	V592 Cas
CEVMKL	$N_H(10^{22}\text{atoms cm}^{-2})$	$0.13^{+0.12}_{-0.06}$	$0.30^{+0.07}_{-0.07}$	$0.3^{+0.2}_{-0.2}$
	α	$1.6^{+2.7}_{-0.4}$	$0.13^{+0.16}_{-0.06}$	$0.6^{+0.7}_{-0.3}$
	$T_{max}(\text{keV})$	$>21^\dagger$	$33.0^{+16.0}_{-14.0}$	$35.5^{+19.7}_{-10.9}$
	K_{CEVMKL}	$9.2^{+7.0}_{-4.8} \times 10^{-4}$	$6.7^{+2.8}_{-1.0} \times 10^{-4}$	$2.3^{+1.1}_{-1.0} \times 10^{-3}$
Power law	$\text{PhoIndex}_{powerlaw}$	$0.82^{+0.07}_{-0.07}$	$0.40^{+0.1}_{-0.3}$	< 1.0
	$K_{powerlaw}$	$2.4^{+1.3}_{-0.20} \times 10^{-4}$	$8.8^{+1.3}_{-4.4} \times 10^{-5}$	$< 7.0 \times 10^{-5}$
	$\chi^2_\nu(\nu)$	1.17 (11)	1.22 (10)	1.17 (9)
	Flux ($10^{-12}\text{erg cm}^{-2}\text{s}^{-1}$)	5.4	5.8	3.4
	Luminosity (10^{32}erg s^{-1})	1.7	4.6	0.5
	Flux _{cevmkl} ($10^{-12}\text{erg cm}^{-2}\text{s}^{-1}$)	0.66	2.3	3.4
	L _{cevmkl} (10^{32}erg s^{-1})	0.2	1.9	0.5
	Flux _{powerlaw} ($10^{-12}\text{erg cm}^{-2}\text{s}^{-1}$)	4.8	2.9	< 1.3
	L _{powerlaw} (10^{32}erg s^{-1})	1.5	2.4	< 0.2

Notes. N_H is the absorbing column, α is the index of the power-law emissivity function ($dEM = (T/T_{max})^{\alpha-1}dT/T_{max}$), T_{max} is the maximum temperature for the CEVMKL model, K_{CEVMKL} is the normalization for the CEVMKL model, $K_{powerlaw}$ is the normalization for the power law model. \dagger A 2σ lower limit of the maximum plasma temperature is stated because the parameter was not constrained in the higher bound limit, the best fitting parameter is $kT_{max}=49.8^{+25.8}_{-25.8}$. Other than the above, all errors are given at 90% confidence limit for a single parameter. The unabsorbed X-ray flux and the luminosities are given in the range 0.2-10.0 keV. Solar abundances have been assumed. For luminosities distances are taken from Table 1.

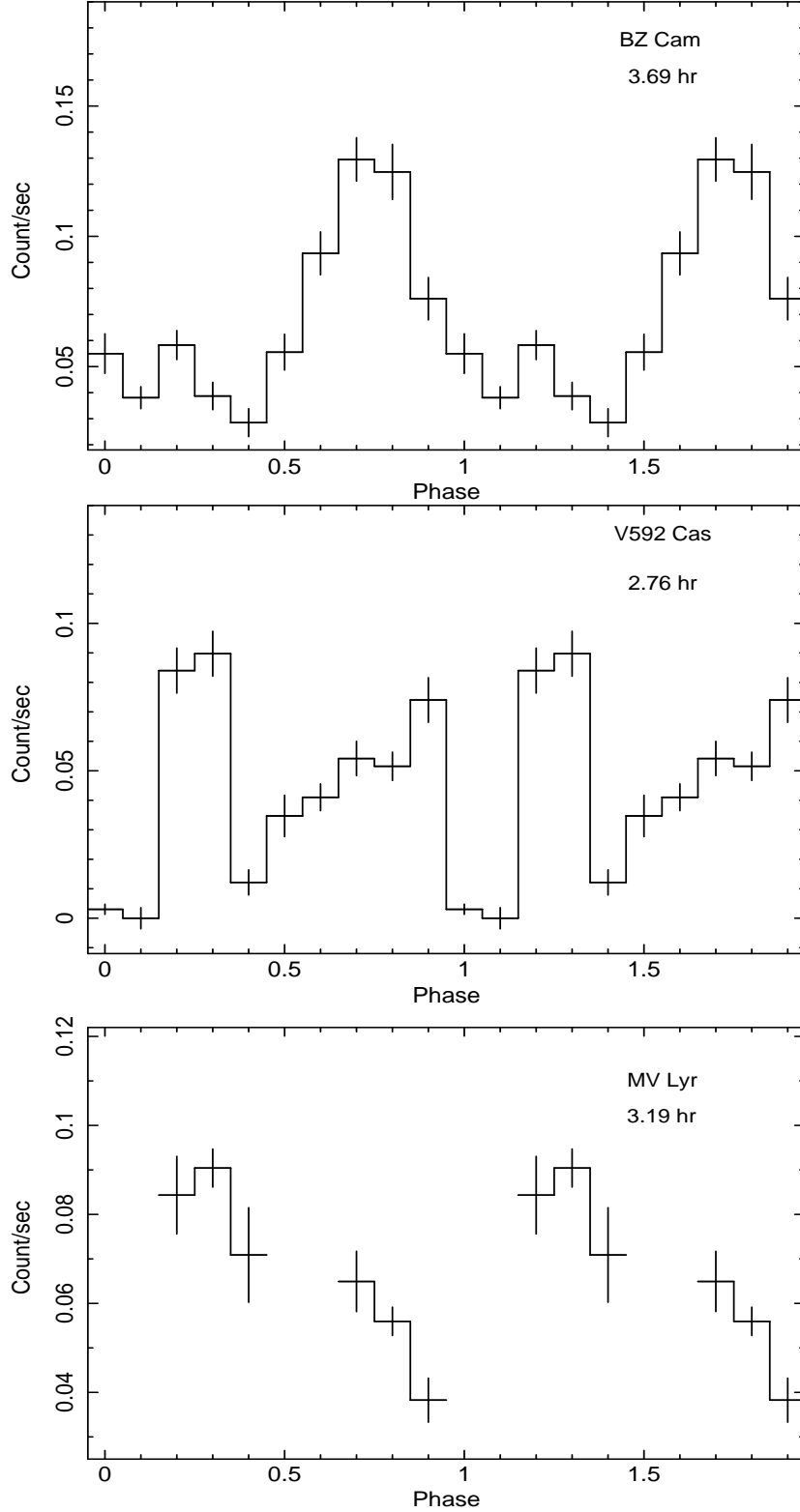


Fig. 1.— Mean *Swift* XRT light curves of BZ Cam, V592 Cas, and MV Lyr folded on their orbital periods (see text for the Ephemerides), respectively. The orbital periods are labeled on the panels. We caution that there is only about one-two cycle of orbital periods for the systems and MV Lyr data does not have full orbital coverage.

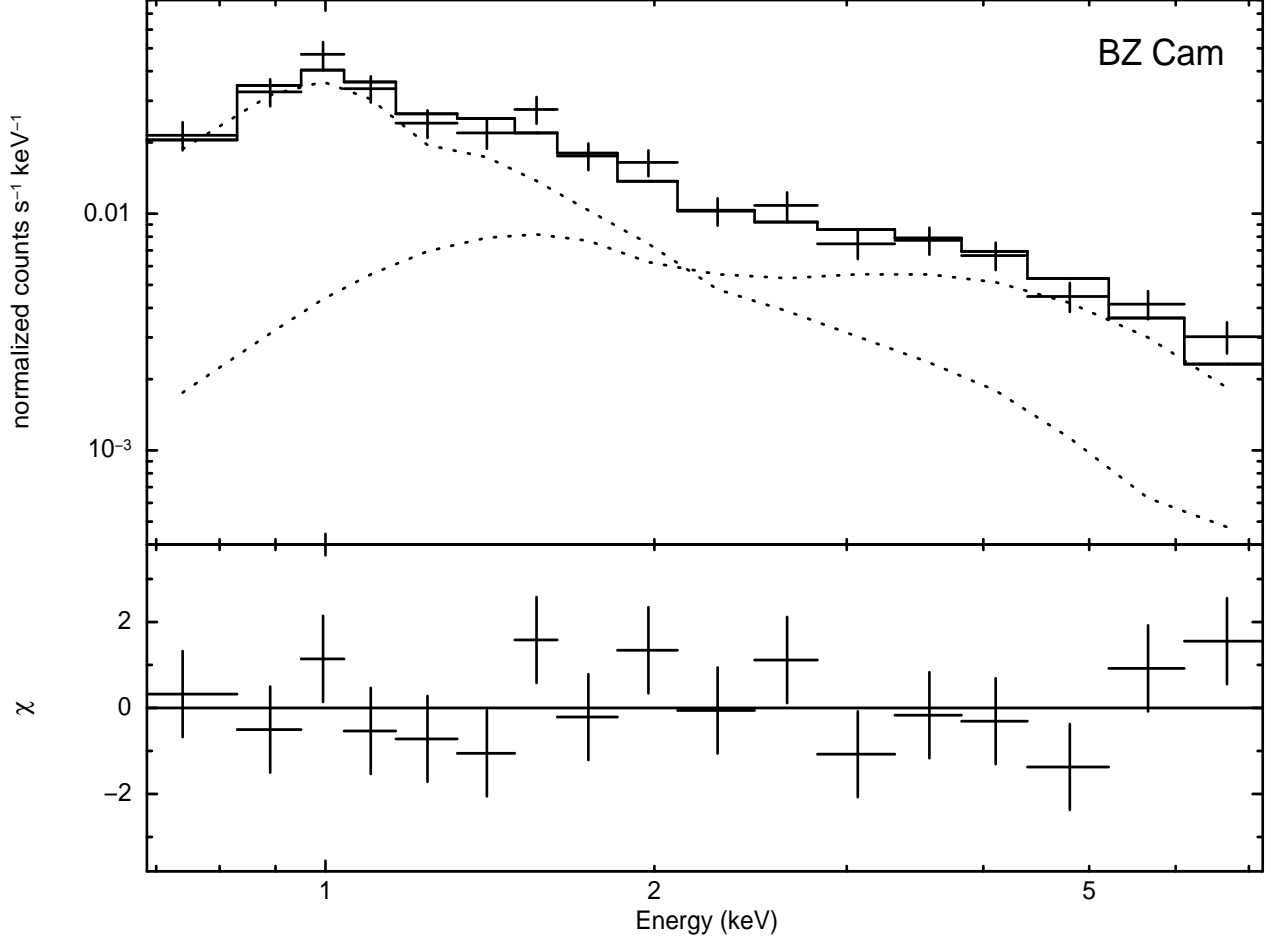


Fig. 2.— The *Swift* XRT spectrum of BZ Cam fitted with ($tbabs*(CEVMKL+POWER)$) model of emission. The dotted lines show the contribution of the two fitted models. The lower panel shows the residuals in standard deviations (in sigma).

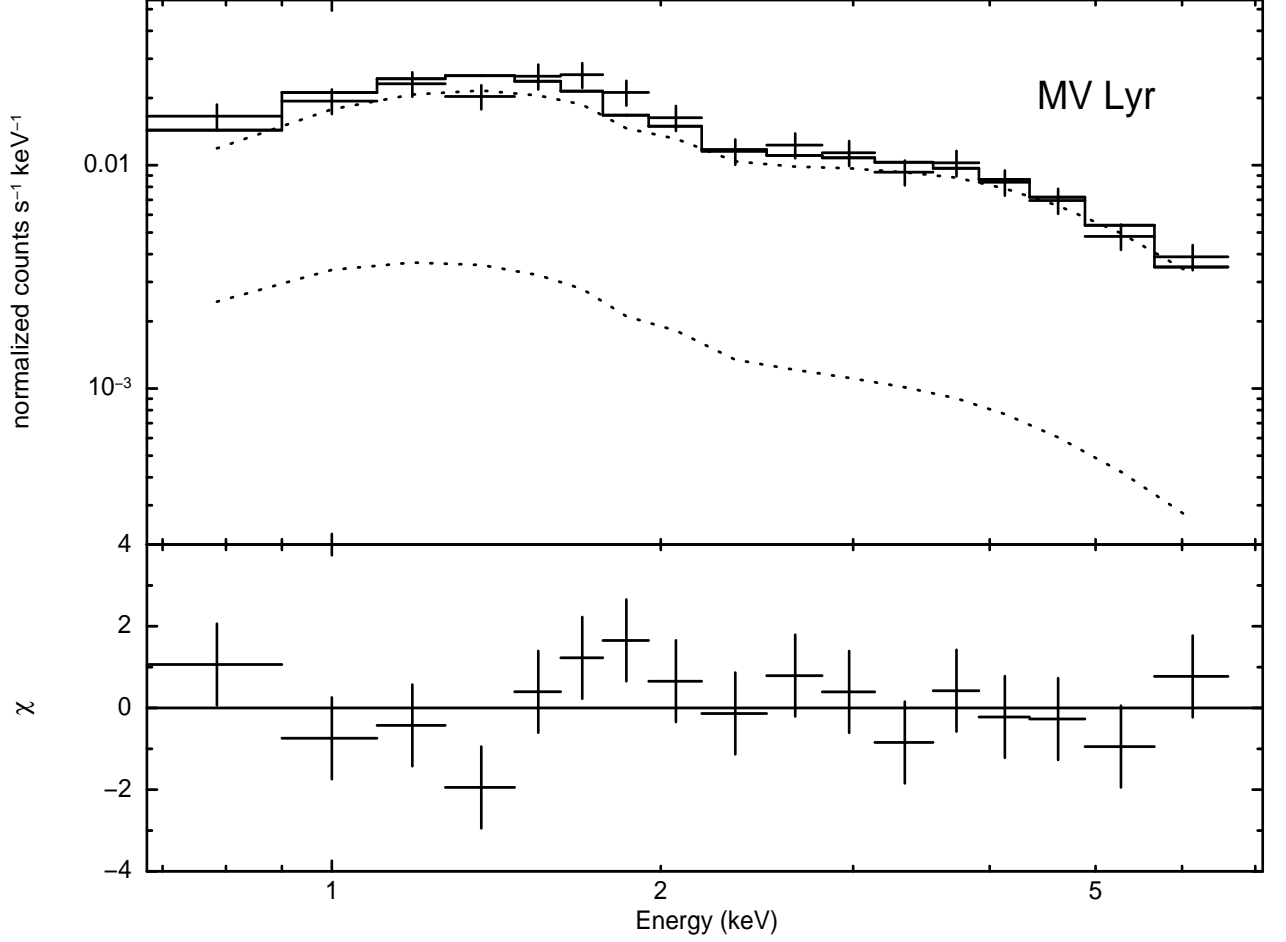


Fig. 3.— The *Swift* XRT spectrum of MV Lyr fitted with ($tbabs*(CEVMKL+POWER)$) model of emission. The dotted lines show the contribution of the two fitted models. The lower panel shows the residuals in standard deviations (in sigma).

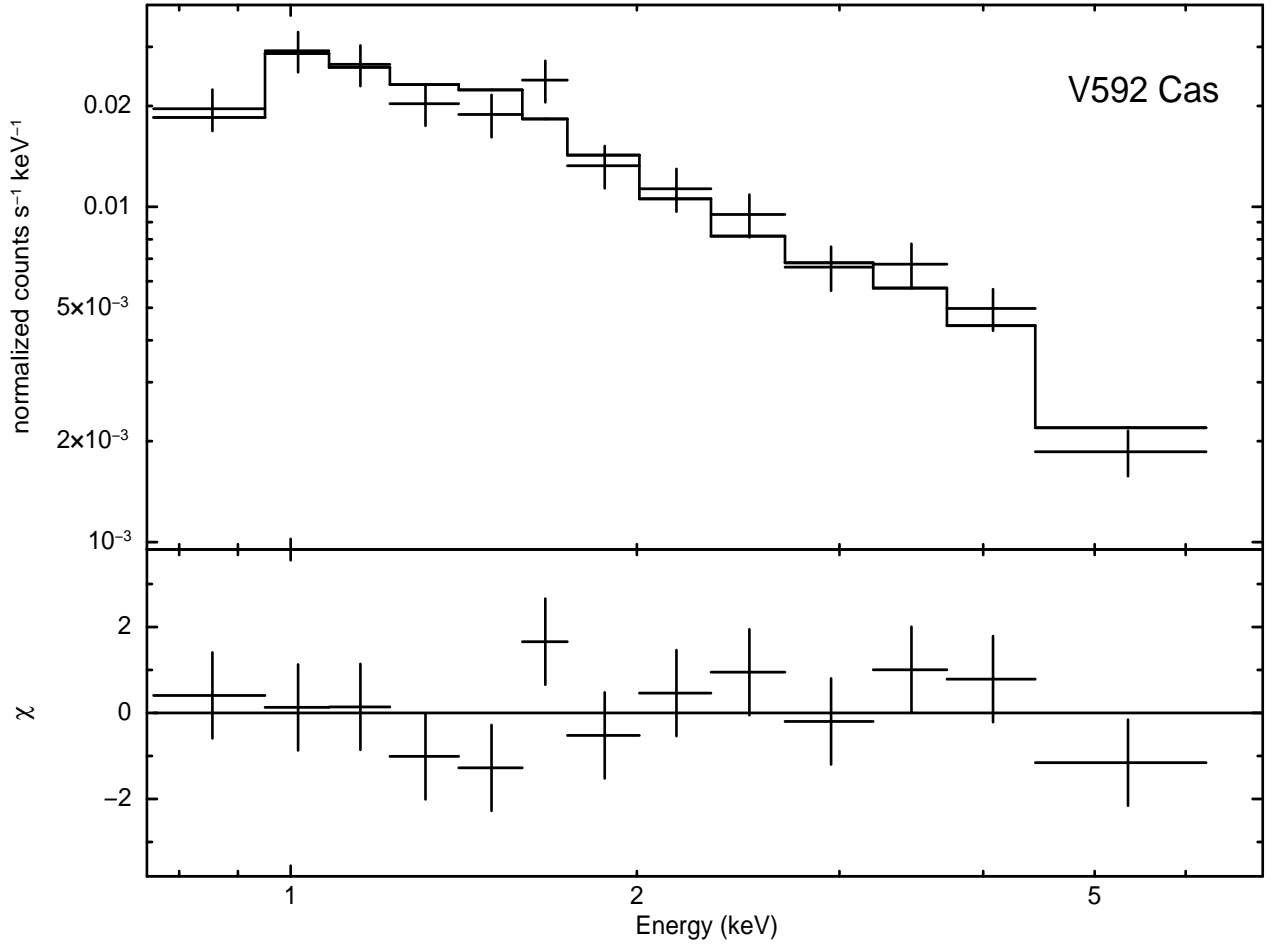


Fig. 4.— The *Swift* XRT spectrum of V592 Cas fitted with (*tbabs**CEVMKL) model of emission. The lower panel shows the residuals in standard deviations (in sigma).